Environmental Science & Technology

Article

pubs.acs.org/est

Gas Purification by Nonthermal Plasma: A Case Study of Ethylene

R. Aerts,*[,†] X. Tu,[‡] W. Van Gaens,[†] J. C. Whitehead,[§] and A. Bogaerts[†]

[†]Research Group PLASMANT, Department of Chemistry, University of Antwerp, Antwerp, Belgium

[‡]Department of Electrical Engineering and Electronics, University of Liverpool, Liverpool, L69 3GJ, United Kingdom

[§]School of Chemistry, The University of Manchester, Oxford Road, Manchester, M13 9PL, United Kingdom

Supporting Information

ABSTRACT: The destruction of ethylene in a dielectric barrier discharge plasma is investigated by the combination of kinetic modeling and experiments, as a case study for plasma-based gas purification. The influence of the specific energy deposition on the removal efficiency and the selectivity toward CO and CO_2 is studied for different concentrations of ethylene. The model allows the identication of the destruction pathway in dry and humid air. The latter is found to be mainly initiated by metastable N_2 molecules, but the further destruction steps are dominated by O atoms and OH radicals. Upon increasing air humidity, the removal efficiency drops by ±15% (from 85% to 70%), but the selectivity toward CO and CO_2 stays more or less constant at 60% and 22%, respectively. Beside CO and CO_2, we also identified acetylene, formaldehyde, and water as byproducts of the destruction process, with concentrations of 1606 ppm, 15033 ppm, and 185 ppm in humid air (with 20% RH), respectively. Finally, we investigated the byproducts generated by the humid air discharge itself, which are the greenhouse gases O_3, N_2O, and the toxic gas NO_2.

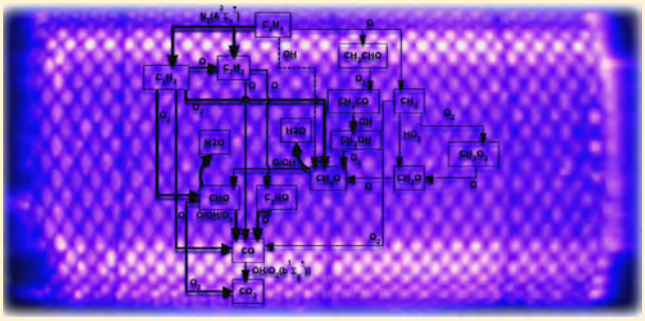

INTRODUCTION

Currently, there is significant interest for the development of nonequilibrium plasma methods for gas purification and abatement. The most common discharge types reported in the literature are dielectric barrier discharges (DBDs), corona discharges, and packed bed surface discharges.[1−4] These methods are based on the formation of a high concentration of chemically active species (i.e., O_3, O, and N_2 metastable molecules) in the polluted gas stream using nonequilibrium low-temperature plasma, without appreciable heating of the treated gas flow. Those generated chemically active species will react with the pollutants and decompose them into less toxic end products (such as CO_2, CO, etc.).[5]

Ethylene (C_2H_4) is an odorless and colorless gas which exists in nature and is generated by human activities, such as engine exhausts, as a petrochemical derivative and in thermal power plants.[6] Moreover, it is used in the food industry to ripen tomatoes, bananas, pears, and a few other fruits postharvest.[7] It is harmful for mankind, causing anesthetic illness and contributes to photochemical smog.[8] Ethylene is an excellent case study hydrocarbon to investigate the destruction mechanism in upcoming gas purification techniques (such as photocatalysis and plasma-assisted catalysis).[9,10]

Numerous papers regarding modeling[11−13] and experimental diagnostics[14,15] indicate the degree of complexity in plasmas for environmental purposes. Both numerical and experimental results are necessary to fully understand the chemical mechanism in the destruction of ethylene. Previously published modeling work regarding volatile organic compounds (VOCs)[16,17] (i.e., formaldehyde, trichloroethylene, etc.) neglected the influence of chemical quenching reactions between metastable N_2 molecules and the hydrocarbon species. However, in our previous work[11] we demonstrated that the contribution of N_2 metastables in the destruction of C_2H_4 could not be neglected. Also Pasquiers and co-workers identified the important role of N_2 metastables in the destruction of different VOCs.[18,19] Therefore, in the present paper, we have expanded our plasma chemistry to fully take into account the effect of metastable N_2 molecules in the destruction process of ethylene in humid air, in a DBD plasma. In our previous work, we mainly focused on the role of electrons in the destruction path, for one pulse and afterglow, and found that they can be neglected. In the present paper, we will investigate in detail the entire reaction pathway, both in dry and humid air, and under more realistic conditions of consecutive pulses. We will also evaluate the effect of humidity on the efficiency of the destruction process and identify the important byproducts. The latter is extremely important for environmental application of this technology.

Received: January 26, 2013
Revised: April 10, 2013
Accepted: May 15, 2013
Published: May 15, 2013

   dx.doi.org/10.1021/es400405c | Environ. Sci. Technol. 2013, 47, 6478−6485

DESCRIPTION OF THE EXPERIMENTS AND THE MODEL

Description of the Experiments. The experimental setup used in this work is a cylindrical DBD reactor consisting of two coaxial fused quartz tubes, both of which are covered by a stainless steel mesh electrode. A more detailed description of the reactor can be found in Tu et al.,[20] although in the present case no catalyst is placed inside the reactor. The gap between both quartz tubes is 3 mm. The reactor volume is 11.4 cm^3, and the experiments are carried out with a flow rate of 1 slm at 300 K, which corresponds to a residence time of 0.684 s. The molecules C_2−C_4 (representing various hydrocarbons with two to four C-atoms), CH_4, H_2, CO, and CO_2 are analyzed by a two-channel microgas chromatograph (GC; Agilent 3000A) equipped with two thermal conductivity detectors (TCD) as described in Tu et al.[20] The molecules NO_2 and N_2O are analyzed by online FTIR spectroscopy (Shimadzu 8300) with a long path IR cell (2.76 m). All the electrical signals are sampled by a four-channel digital oscilloscope (Agilent DSO6014A, 2 GHz). A LABVIEW control system is used for the online measurement of the discharge power by the area calculation of the Q-U Lissajous figure.

Description of the Model and the Chemistry. The model used in this work is a global kinetic (0D) model, called global_kin, developed by M. Kushner and co-workers.[21] The model includes an online Boltzmann solver for the electron-induced reactions. It constructs lookup tables for the reaction rate coefficients versus the mean electron energy, based on the corresponding cross sections. Furthermore, a gas-phase kinetics module calculates the time-evolution of the density of every species and of the electron energy at a fixed temperature of 350 K. This temperature is chosen 50 K higher than the experimental temperature of the gas flow, to take into account local overheating in the microdischarge itself, which is reported to be around 50 K.[22,23] Finally, an extra module is recently added to investigate the production and loss of each species from each individual reaction. More details about this module can be found in Aerts et al.[24]

The chemistry set used in this model can be divided into two subsets. The first subset is for the background gas, i.e., humid air ($21 - x/2\%$ O_2, $79 - x/2\%$ N_2, where x = % H_2O), and the second subset represents the hydrocarbon chemistry. The details of the humid air chemistry set are reported by Van Gaens et al.,[25] and a description of the initially dominant reactions in (humid) air can be found in the work of Kossyi and co-workers.[26] The hydrocarbon set is based on the chemistry published by Snoeckx et al.[27] and Aerts et al.,[11] but it is extended with chemical reactions between N_2 metastable molecules and hydrocarbon species. In total the model contains 113 chemical species and 1639 reactions.

RESULTS AND DISCUSSION

Description of the Power Deposition. DBDs mostly operate in filamentary mode, which can be observed by the many short peaks in the electrical current waveform as shown in Figure 1. These filaments (streamers) are spread in volume and time, making it very difficult to model in a typical (continuum) plasma model. By using a zero-dimensional kinetic model, this problem can be overcome as follows. The power deposition is defined as a pulse of 15 ns, which corresponds to the typical lifetime of such a filament.[28] The maximum power deposition in this pulse is chosen to obtain typical values for electron temperature and electron density, as reported in the literature.[28] By simulating a number of these consecutive discharge pulses, the filamentary behavior of the DBD can be mimicked.

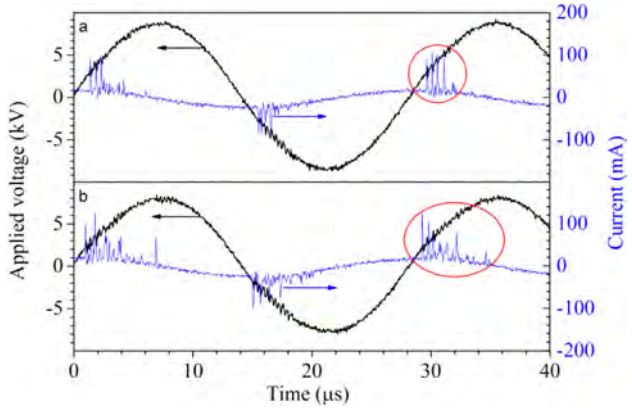

Figure 1. Measured voltage (left y-axis) and current (right y-axis) as a function of time, for a specific energy deposition (SED) of 1.2 J/cm^3 (a) and 2.4 J/cm^3 W (b), in the case of 3500 ppm C_2H_4 in dry air. The red circles indicate that the number of microdischarge pulses increases as a function of SED (or power).

Although in reality, a large number of filaments occur per half cycle (see Figure 1), the ethylene molecules will not pass all these filaments, as they are spread in volume. The exact number of filaments that a typical ethylene molecule will pass when flowing through the reactor is not known. Therefore, we have subdivided the total energy deposition in the experiment into a number of triangular pulses (filaments). The individual pulse energy and the number of pulses were adapted to match the electron temperature adopted from the literature and the experimentally obtained electron density, making sure that the total simulated energy deposition is the same as the total energy deposition in the experiment. If the obtained electron temperature and density have realistic values, the other plasma characteristics, including the densities of the other plasma species, are most probably also realistic. More details about this method can also be found in Aerts et al.[24] and Snoeckx et al.[27]

It should be mentioned that by increasing the specific energy deposition (SED) in the experiments the number of filaments visually increases, and as a result also the number of peaks in the current waveform becomes higher. Figure 1 illustrates the increase in number of current pulses for a rise in SED from 1.2 to 2.4 J/cm^3, for 3500 ppm ethylene in dry air.

In Figure 2, the values of electron density as obtained from the model and the experiment are plotted as a function of SED, together with the number of simulated discharge pulses through which the ethylene molecules will pass when flowing through the reactor. Note that the electron density obtained from the experiment is not measured directly but is simply estimated from the electrical current density, as follows: $n_e = J/(E\mu_e e)$, where J is the experimental current density, μ_e is the drift mobility for electrons, adopted from Nielsen et al.,[29] E is the electric field, estimated from the ratio of breakdown voltage versus gap, and e is the elementary charge (1.602×10^{-19}).[20,30] The figure shows that both the experimental and calculated electron density drop slightly upon increase of the SED (or the discharge power), and as a result, the number of pulses (filaments) should increase, to correspond to the rise in SED.

Effect of SED on the Ethylene Destruction Process. In this section we will discuss the effect of the SED on the removal

dx.doi.org/10.1021/es400405c | Environ. Sci. Technol. 2013, 47, 6478−6485

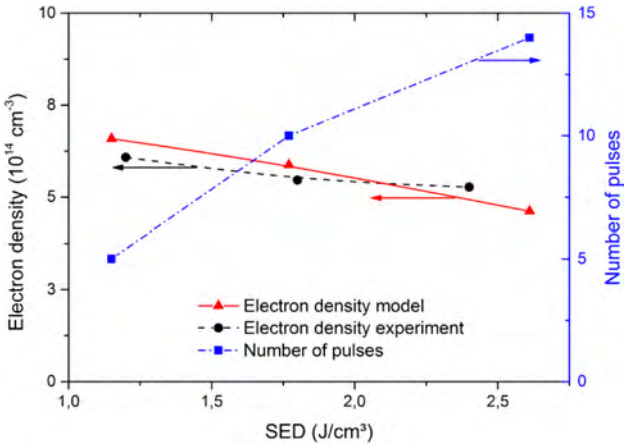

Figure 2. Electron density, both calculated from the model and estimated from the experiment, as a function of the specific energy deposition (SED) (left *y*-axis), as well as the total number of microdischarge pulses assumed in the simulations for a residence time of 0.684 s (right *y*-axis), for 3500 ppm C_2H_4 in dry air.

efficiency (RE) and on the selectivity of CO (S_{CO}) and CO_2 (S_{CO2}), which are defined as:

$$\text{RE}\ (\%) = \frac{C_2H_{4(\text{inlet})} - C_2H_{4(\text{outlet})}}{C_2H_{4(\text{inlet})}} \times 100\%$$

$$S_{CO}\ (\%) = \frac{\text{moles of CO produced}}{2 \times \text{moles of } C_2H_4 \text{ converted}} \times 100\%$$

$$S_{CO_2}\ (\%) = \frac{\text{moles of } CO_2 \text{ produced}}{2 \times \text{moles of } C_2H_4 \text{ converted}} \times 100\%$$

The calculations and experiments are performed for 3500 ppm, 8700 ppm, and 13700 ppm ethylene in dry air, in a range of discharge power from 20 to 40 W, corresponding to an SED between 1.2 and 2.4 J/cm^3. Figure 3 illustrates the calculated and measured RE, S_{CO}, and S_{CO2} for these three ethylene concentrations as a function of SED. The RE increases with rising energy deposition, both in the experiments and in the simulations. This is attributed to the larger concentrations of "activating" air species (such as metastable N_2 molecules and O atoms; see below), which destroy the C_2H_4 molecules. It is also clear from Figure 3a that the RE is the highest at low concentrations of C_2H_4, because the possibility that all C_2H_4 molecules can react with "activating" air species also increases. Nevertheless, at an SED of 2.5 J/cm^3, the RE is almost 100% for all C_2H_4 concentrations. Note that the model predicted a somewhat lower RE for the 13700 ppm case compared to the experiment, but in general, the agreement is quite satisfactory. The removal efficiency was previously benchmarked with other VOCs.[11] However, it should be realized that ethylene is quite simple to destroy in a plasma compared to other (e.g., aromatic) VOCs, as can be seen from the high removal efficiencies close to 100% presented in the literature for different discharge types,[2,6] for inlet concentrations ranging from 100 ppm till 3%.

Figure 3b,c shows that there is also a reasonable agreement between the model and experimental results for the CO and CO_2 selectivity. An increase in SED does not influence the CO selectivity to a large extent, which is more or less constant at ±50−60%. The selectivity toward CO_2 is on the order of 10−40%, increasing slightly upon higher SED, which is more

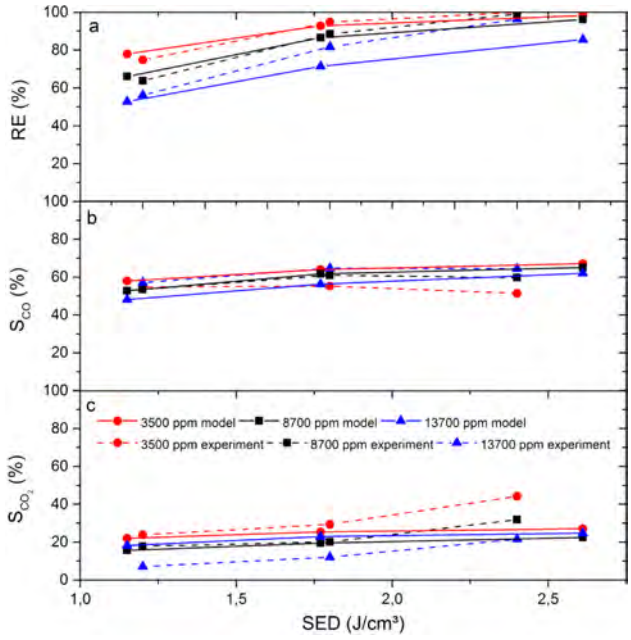

Figure 3. Comparison between calculated (solid lines) and measured (dashed lines) removal efficiency (RE) (a), and selectivities toward CO and CO_2, i.e., S_{CO} (b) and S_{CO2} (c), at different concentrations of C_2H_4 in dry air and as a function of the SED.

apparent from the experiments than from the simulations (see Figure 3c). This can be explained by the increasing number of pulses upon a rise in the SED, increasing the possibility to convert the byproducts into CO_2. The reason why the CO selectivity remains constant is that it is more efficiently created from the byproducts at higher SED, but at the same time, it is also more efficiently oxidized into CO_2, so that the net production of CO remains constant. Furthermore, for a lower concentration of ethylene, the CO selectivity drops slightly, whereas the CO_2 selectivity increases, indicating that the destruction process becomes "more clean". In general, we can conclude that the destruction of C_2H_4 in a DBD is predicted by our model in reasonable agreement to the experiment, both for different C_2H_4 concentrations and for different specific power depositions. Most of the C_2H_4 is converted to CO as can be seen from the selectivity toward CO (±60%). Moreover, at high values of SED and at low C_2H_4 concentrations, the selectivity toward CO_2 reaches ±40%. In this case almost all C_2H_4 is converted into CO and CO_2. At lower values of SED and higher C_2H_4 concentrations, the selectivity toward CO_2 drops to ±10−20%, indicating that some byproducts are formed, as will be elaborated below.

Identification of the Destruction Pathway. As the calculated RE and selectivities of CO and CO_2 correspond well with the measured values, both in absolute values as well as the trends as a function of SED and C_2H_4 concentrations, the model can be used to elucidate the destruction pathway of C_2H_4 in a DBD in dry and humid air, which is illustrated in Figure 4. The thickness of the arrows indicates the importance of the various reaction paths. Note that the latter might vary a bit, depending on the values used for some of the rate coefficients (cf., the deviations found for different literature values; see Supporting Information). Nevertheless, in view of the good agreement between calculated and measured results, we are quite confident that this reaction pathway presents a realistic picture.

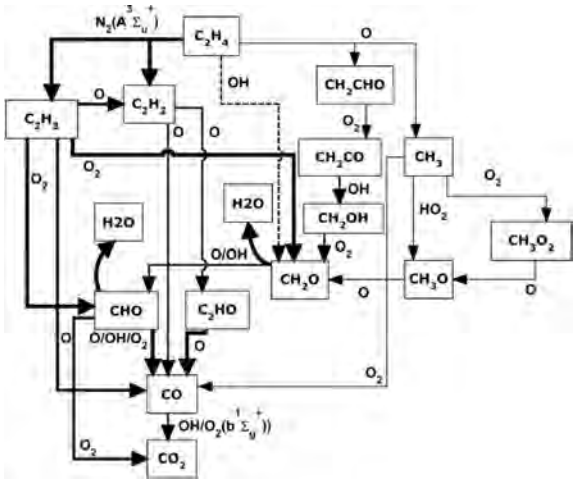

Figure 4. Ethylene destruction pathway in dry and humid air, as elucidated by the model. The thickness of the arrows indicates the importance of the various reaction paths. The pathway is more or less similar in both dry and humid air, except for some extra destruction through OH radicals in humid air, as indicated by the dashed arrow in the figure.

In general, both in dry and humid air, two main destruction mechanisms can be distinguished, i.e., upon collision with metastable N_2 molecules (especially $N_2(A^3\sum_u^+)$) and with O atoms, but the first one appears to be most important, producing vinyl radicals (C_2H_3) and acetylene molecules (C_2H_2); see Figure 4. The fact that acetylene has a triple bond and a high ionization energy of 11.4 eV[31] makes it very difficult to destroy, and as a result, acetylene will be one of the byproducts besides CO and CO_2 (see further). Nevertheless, it can also be further oxidized with O toward C_2HO and finally toward CO and CO_2.

A more important oxidation path, especially in dry air, proceeds through the C_2H_3 radical, which will be oxidized to CHO radicals and formaldehyde (CH_2O):[32]

$$C_2H_3 + O_2 \rightarrow CHO + CH_2O \quad (k = 9.0 \times 10^{-12}\ cm^3/s) \qquad (R1)$$

In addition, it can also react with O to CO and CH_3, or to acetylene and OH:[33]

$$C_2H_3 + O \rightarrow CO + CH_3 \quad (k = 1.25 \times 10^{-11}\ cm^3/s) \qquad (R2)$$

$$C_2H_3 + O \rightarrow C_2H_2 + OH \quad (k = 1.25 \times 10^{-11}\ cm^3/s) \qquad (R3)$$

Note that in Figure 4, only arrows are drawn toward CO and C_2H_2 and not to CH_3 and OH, as the latter species are radicals which react further, whereas CO and C_2H_2 are obtained as byproducts.

Hübner et al. also reported formaldehyde as one of the byproducts in their experimental work on ethylene destruction.[34] However, formaldehyde is also a VOC which can be destroyed in plasma.[19,35,36] The latter is also observed in our model, where the formaldehyde concentration decreases for an increasing number of pulses. Indeed, most of the formaldehyde will be further oxidized to CHO by O or OH, which have their highest density shortly after each pulse:[32,37]

$$CH_2O + O \rightarrow CHO + OH \quad (k = 1.78 \times 10^{-11}(T/298\ K)e^{(-1390[K]//T)}\ cm^3/s) \qquad (R4)$$

$$CH_2O + OH \rightarrow CHO + H_2O \quad (k = 8.2 \times 10^{-12}e^{(40[K]/T)}\ cm^3/s) \qquad (R5)$$

Reaction of CHO with O, O_2, or OH eventually leads to the formation of CO and CO_2, as shown in Figure 4.

Finally, the oxidation process from CO to CO_2 can be assigned to reaction with $O_2(b^1\sum_g^+)$ metastable molecules or OH radicals, the latter path being more important:[32,38]

$$CO + O_2(b^1\sum_g^+) \rightarrow CO_2 + O \quad (k = 3.7 \times 10^{-15}\ cm^3/s) \qquad (R6)$$

$$CO + OH \rightarrow CO_2 + H \quad (k = 5.4 \times 10^{-14}(T/298\ K)^{1.50}e^{(250[K]/T)}\ cm^3/s) \qquad (R7)$$

The paths presented in the right side of the figure contribute for only a few percent to the oxidation pathway, as indicated by the thinner arrows, and they are therefore not discussed in detail here. They become slightly more important in humid air.

The air humidity does not really influence the dominant reaction pathways, but it does affect the relative importance of the different reagents, i.e., OH, O, and O_2. The higher OH density in humid air introduces an extra reaction path (see dashed line in Figure 4), producing formaldehyde. The effect of the air humidity on the efficiency of the destruction process will be discussed in detail in the next section.

We can summarize the reaction pathway as follows: (1) The initial destruction of ethylene in dry air is dominated by metastable N_2 molecules and to a lower extent by O atoms. (2) The initial destruction of ethylene in humid air is similar to that in dry air, but the OH radicals give rise to an extra destruction path. (3) The further destruction path to CO and CO_2 in both dry and humid air is fully controlled by O atoms and OH radicals, and the contribution of the OH radicals increases with increasing humidity.

Effect of the Air Humidity on the Ethylene Destruction Process. As mentioned in the previous section, an increase in air humidity does not influence the reaction pathway to a large extent, as most of the destruction is initiated by N_2 metastable molecules. Figure 5 presents the effect of air humidity on the RE and on the selectivity toward CO and CO_2, for an energy deposition of 1.8 J/cm^3 and 8700 ppm C_2H_4 in air. The calculations were performed for relative humidity between 0% and 99%, whereas the experiments could only be carried out until 20% humidity, but at least in this range the agreement between experiment and model is quite good. Our calculations predict that the selectivity toward CO and CO_2 does not change significantly upon increasing humidity. However, the RE drops by about 15% when the humidity rises from 0% to 99%. This can be explained by the drop in densities of the O atoms and metastable N_2 molecules at the maximum of the pulse (i.e., from 8.8×10^{16} cm^{-3} to 4.8×10^{16} cm^{-3} for the O atoms, and from 6.8×10^{16} cm^{-3} to 4.1×10^{16} cm^{-3} for the metastable N_2 molecules). The humidity might influence the formation of other byproducts (see below), but this effect will be minor, as the CO and CO_2 selectivities remain approximately constant.

dx.doi.org/10.1021/es400405c | Environ. Sci. Technol. 2013, 47, 6478−6485

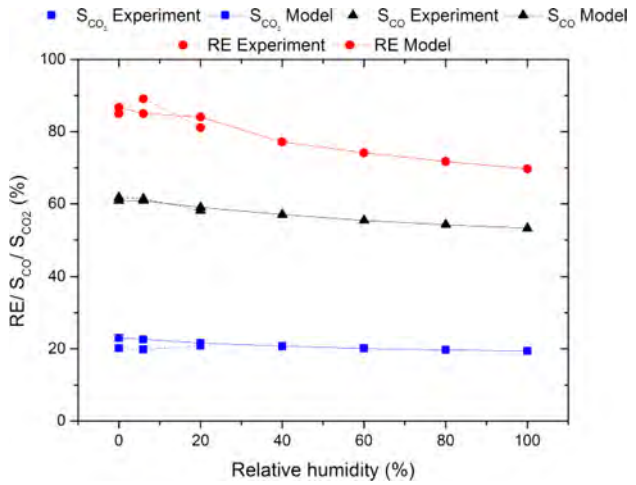

Figure 5. Comparison between calculated (solid lines) and measured (dashed lines) RE (red; circle), S_{CO} (black; triangle), and S_{CO_2} (blue; square), as a function of the relative air humidity, for an energy deposition of 1.8 J/cm^3 at 8700 ppm C_2H_4 in air.

Figure 6 illustrates the calculated densities (in ppm) of the most common byproducts besides CO and CO_2 as a function

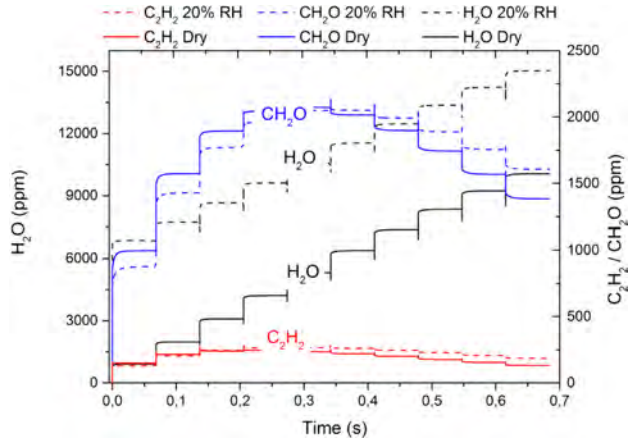

Figure 6. Calculated concentrations of H_2O (left axis), CH_2O, and C_2H_2 (right axis), formed as byproducts in C_2H_4 destruction, as a function of time during 10 consecutive microdischarge pulses, in the case of humid air with 20% RH (dashed lines) and dry air (solid lines), for a total energy deposition of 1.8 J/cm^3 at 8700 ppm C_2H_4 in air.

of time, for 10 consecutive pulses (i.e., microdischarge filaments) with an interpulse time of ±0.0684 s. Only the calculated concentrations of the byproducts could be obtained. Indeed, we could not separate the C_2H_2 and C_2H_4 peaks on the GC. However, a rough estimation by FTIR indicated ±26 ppm C_2H_2, which is somewhat lower than the calculated result (see Figure 6 and below). We could not detect CH_2O on the GC or the FTIR, possibly because this species might be condensed after the plasma reactor. The results are shown for an energy deposition of 1.8 J/cm^3 and 8700 ppm C_2H_4, both in humid air with 20% relative humidity (RH) and in dry air. The concentrations of CH_2O, H_2O, and C_2H_2 after a residence time of 0.684 s, i.e., when the gas flows out of the reactor, amount to 1606 ppm, 15033 ppm, and 185 ppm, respectively, in humid air (with 20% RH), and to 1382 ppm, 10057 ppm, and 131 ppm, respectively, in dry air. This corresponds to selectivities toward CH_2O and C_2H_2 of 11% and 3%, respectively, in the humid air case (and slightly lower in dry air). At these conditions, the selectivities toward CO and CO_2 are calculated to be 60% and 22% (see Figure 5), so that the sum of these selectivities amounts to 96%; the remaining 4% goes to methane, formic acid, and ketene. Note that the selectivity toward H_2O is not included in these calculations, as the selectivities are obtained with respect to the C atoms in C_2H_4, and H_2O does not contain C atoms.

Figure 6 shows that the CH_2O, H_2O, and C_2H_2 densities exhibit a rise (or a drop) at each pulse, whereas they remain more or less constant in the interpulse time. Furthermore, the H_2O density keeps on increasing for the consecutive pulses, whereas the CH_2O and C_2H_2 densities go over a maximum after the fifth pulse. The latter behavior can be explained because more chemically active species (i.e., O_3, O, and N_2 metastable molecules) are available at this time to destroy CH_2O and C_2H_2. We have found that the C_2H_4 removal progresses as a function of time, and the densities of CH_2O and C_2H_2 become comparable to the C_2H_4 density, and at that point the chemically active species also yield the destruction of CH_2O and C_2H_2.

H_2O, on the other hand, will be consumed by electron impact dissociation and by vibrational excitation during each pulse, whereas after the pulse, it is produced again by decay of the vibrationally excited species and by reaction of OH radicals with hydrocarbon species (e.g., eq R5 above). However, an extra hydrogen source is necessary to explain the stepwise increasing H_2O density. The explanation can be found in the indirect production of H_2O by the destruction of ethylene and its byproducts. The reactions between hydrocarbon species and O atoms will produce OH radicals (e.g., by eq R3), and those OH radicals will then react with hydrocarbon species in a second reaction (e.g., by eq R5).

In general, a higher humidity does not result in different byproducts formed, but the concentration of formaldehyde increases by 224 ppm for a humidity of 20% compared to dry air. This difference is attributed to the higher density of OH radicals, which results in a new destruction path, as discussed above. Note that the time-integrated rate of the reaction:[39]

$$C_2H_4 + OH \rightarrow CH_2O + CH_3 \quad (k = 1.6 \times 10^{-15}\ cm^3/s) \qquad (R8)$$

increases by 1 order of magnitude, i.e., from 10^{16} cm^{-3} to 10^{17} cm^{-3}, when the RH rises from 0% to 90%. However, this rate is still 3 orders of magnitude lower than the integrated rates of the reactions with metastable N_2 molecules, explaining why the effect of humidity is not significant. The effect of humidity on the C_2H_2 density is even smaller, and the minor drop in density can be assigned to the drop in metastable N_2 density, as most of the C_2H_2 production is caused by the N_2 metastable destruction of ethylene (see Figure 4 above). Finally, the effect on the H_2O concentration is simply due to the extra water introduced in the humid air, but the H_2O production itself does not change, as shown in Figure 6.

Production of O_3, NO_2, HNO_2, HNO_3, and N_2O. Not only are hydrocarbon byproducts an issue in plasma destruction of VOCs, but also the production of O_3, NO_2, HNO_2, and N_2O in the carrier gas (air) must be considered. In Table 1 the concentrations of produced O_3, NO_2, HNO_2, and N_2O species are listed, after treating 3500 ppm C_2H_4 in dry air with an energy deposition between 1.2−2.4 J/cm^3.

dx.doi.org/10.1021/es400405c | Environ. Sci. Technol. 2013, 47, 6478−6485

Table 1. Calculated Concentrations of O_3, NO_2, N_2O, and HNO_2 Formed as Byproducts in the Destruction of 3500 ppm C_2H_4 in Dry Air, for Different Values of SED[a]

	species			
SED (J/cm^3)	O_3(ppm)	NO_2 (ppm)	N_2O (ppm)	HNO_2 (ppm)
1.2	632	3 (165)	214 (52.5)	776
1.8	1089	6 (198)	287 (74)	996
2.4	3043	22 (225)	358 (77)	1249

[a]The measured values of the NO_2 and N_2O concentrations are also indicated between parentheses.

DBDs have been known as ozone producers for many years.[40] It is, therefore, not unexpected that O_3 is also formed as a byproduct in VOC destruction in air. As follows from Table 1, the created O_3 concentration is on the order of (several) 1000 ppm, hence the same order of magnitude as the C_2H_4 concentration to be destroyed. Moreover, it increases drastically with SED, which is directly related to the higher O atom density, producing more O_3 upon three-body recombination between molecular and atomic oxygen.[41] We could not detect any characteristic peak of O_3 on the FTIR, but we suspect that ozone is decomposed on the warm reactor walls and on the tubing to the FTIR. Second, it is also possible that we have reached the critical point of discharge poisoning by both working at higher power and by heating the electrodes.[28]

For the NO_2 and N_2O concentrations, both the calculated and measured values are listed. The calculated NO_2 concentration is 1−2 orders of magnitude lower than the measured values. This might be attributed to some missing reactions (or an error in some rate coefficients) in the NO_x plasma chemistry, which was, of course, not the main purpose of this work. However, it could also be an error in the experiment, due to the difference between the time of measurement and the residence time of the gas in the reactor. Indeed, the NO_2 concentration is still increasing at the end of our simulation, or in other words at the end of the reactor; therefore, it is likely that the actual NO_2 concentration would be higher at the place of measurement. The dissociation of HNO_4 can be found responsible for this production:[42]

$$HNO_4 + M \rightarrow HO_2 + NO_2 \quad (k = 1.3 \times 10^{-20}\ \text{cm}^3/\text{s}) \qquad \text{(R9)}$$

The calculated N_2O concentration is about a factor of 4 higher than the measured values, which is still reasonable, in view of the complex plasma chemistry. Moreover, in the literature, the NO_2 concentration was typically reported to be lower than the N_2O concentration,[6,34] which corresponds to our modeling results. Another explanation for the different values could be temperature effects at the wall of the reactor, caused by ohmic heating in the electrode, and therefore the chemistry will locally be different from the bulk chemistry. Within this discussion we should comment that an experimental measurement of the atomic oxygen concentration would provide us a more detailed validation.

Furthermore, the model predicts the production of HNO_2 and small quantities of HNO_3, which is not directly expected in dry air, although water is produced during the destruction of ethylene. The destruction of water will then produce OH and HO_2 radicals which will react with NO or NO_2, producing HNO_2 and HNO_3. The ratio between HNO_2 and HNO_3 will eventually be controlled by the reaction:[43]

$$HNO_3 + NO_2^- \rightarrow NO_3^- + HNO_2 \quad (k = 1.6 \times 10^{-9}\ \text{cm}^3/\text{s}) \qquad \text{(R10)}$$

which explains why we calculated the largest density for HNO_2 and not for HNO_3. We should, however, keep in mind that in this case the ratio between HNO_2 and HNO_3 is strongly dependent on the error on the rate coefficient. We were not able to detect any peaks of HNO_2 or HNO_3 on the FTIR, but it could be possible that they condense in the tubing to the FTIR, together with water.

Finally, similar to that for O_3, the NO_2, N_2O, and HNO_2 concentrations increase at higher SED, which can again be explained by the increasing density of O atoms and metastable N_2 species ($N_2(A^3\sum_u^+)$) in the discharge, giving rise to the following reactions:[32,44]

$$O + O_2 \rightarrow O_3 \quad (k = 6.0 \times 10^{-34}(T/298\ \text{K})^{-2.8}\ \text{cm}^3/\text{s}) \qquad \text{(R11)}$$

$$O + NO + M \rightarrow NO_2 + M \quad (k = 1.0 \times 10^{-31}(T/298\ \text{K})^{-1.60}\ \text{cm}^6/\text{s}) \qquad \text{(R12)}$$

$$N_2(A^3\sum_u^+) + O_2 \rightarrow N_2O + O \quad (k = 7.8 \times 10^{-14}\ \text{cm}^3/\text{s}) \qquad \text{(R13)}$$

Furthermore, an increase in the NO_2 density will then stimulate the production of HNO_2 and HNO_3.

In conclusion, the destruction of ethylene in a DBD goes side by side with the production of O_3, NO_2, HNO_2, HNO_3, and N_2O, in concentrations which are not negligible to the C_2H_4 concentration to be destroyed. This should of course be avoided. In general, all end products of C_2H_4 destruction can be categorized as sources of photochemical smog (i.e., NO_2, HNO_2, CO, and VOCs (e.g., formaldehyde)) or greenhouse gas emissions (i.e., O_3, N_2O, and CO_2, where N_2O should be considered as the most harmful in this group, because of its global warning potential of 289 (based on 20 years)[45]). In our opinion, plasma technology can therefore only be viable for VOC destruction purposes if combined with catalysis, i.e., so-called plasma catalysis, to minimize the outlet O_3 and NO_x concentrations, produced by the plasma itself.[9] This will be investigated in our future work regarding the application of plasmas for environmental applications.

■ ASSOCIATED CONTENT

Ⓢ Supporting Information

Reactions included in the model between metastable N_2 molecules and hydrocarbon species, as well as their corresponding rate coefficients and the references from where these data were adopted. This material is available free of charge via the Internet at http://pubs.acs.org.

■ AUTHOR INFORMATION

Corresponding Author

*Phone: +32 (0)3 265 23 60; e-mail: robby.aerts@ua.ac.be.

Author Contributions

The manuscript was written through contributions of all authors. All authors have given approval to the final version of the manuscript. All authors contributed equally.

Notes

The authors declare no competing financial interest.

■ ACKNOWLEDGMENTS

We are very grateful to M. Kushner and group members from providing the global_kin code and useful advice. This work was carried out using the Turing HPC infrastructure at the CalcUA core facility of the Universiteit Antwerpen, a division of the Flemish Supercomputer Center VSC, funded by the Hercules Foundation, the Flemish Government (department EWI), and the Universiteit Antwerpen. We also acknowledge financial support from an IOF-SBO project of the University of Antwerp. The experimental work performed at Manchester was supported by the UK EPSRC.

■ REFERENCES

(1) Xia, L.; Huang, L.; Shu, X.; Zhang, R.; Dong, W.; Hou, H. Removal of ammonia from gas streams with dielectric barrier discharge plasmas. *J. Hazard. Mater.* **2008**, *152*, 113−9.

(2) Chavadej, S.; Saktrakool, K.; Rangsunvigit, P.; Lobban, L.; Sreethawong, T. Oxidation of ethylene by a multistage corona discharge system in the absence and presence of Pt/TiO_2. *Chem. Eng. J.* **2007**, *132*, 345−353.

(3) Ding, H.-X.; Zhu, A.-M.; Yang, X.-F.; Li, C.-H.; Xu, Y. Removal of formaldehyde from gas streams via packed-bed dielectric barrier discharge plasmas. *J. Phys. D: Appl. Phys.* **2005**, *38*, 4160−4167.

(4) Sun, Y.; Chmielewski, A.Organic pollutants treatment from air using electron beam generated nonthermal plasma—overview. In *Organic Pollutants Ten Years After the Stockholm Convention - Environmental and Analytical Update*; InTech North America: New York, 2012

(5) Chen, H. L.; Lee, H. M.; Chen, S. H.; Chang, M. B.; Yu, S. J.; Li, S. N. Removal of volatile organic compounds by single-stage and two-stage plasma catalysis systems: a review of the performance enhancement mechanisms, current status, and suitable applications. *Environ. Sci. Technol.* **2009**, *43*, 2216−27.

(6) Harling, A. M.; Glover, D. J.; Whitehead, J. C.; Zhang, K. Novel method for enhancing the destruction of environmental pollutants by the combination of multiple plasma discharges. *Environ. Sci. Technol.* **2008**, *42*, 4546−50.

(7) Burg, S. P.; Burg, E. A. Role of Ethylene in Fruit Ripening. *Plant Physiol.* **1962**, *37*, 179−89.

(8) Li, J.; Ma, C.; Xu, X.; Yu, J.; Hao, Z.; Qiao, S. Efficient elimination of trace ethylene over nano-gold catalyst under ambient conditions. *Environ. Sci. Technol.* **2008**, *42*, 8947−51.

(9) Hussain, M.; Bensaid, S.; Geobaldo, F.; Saracco, G.; Russo, N. Photocatalytic degradation of ethylene emitted by fruits with TiO_2 Nanoparticles. *Ind. Eng. Chem. Res.* **2011**, *50*, 2536−2543.

(10) Francke, K. Plasmacatalytic processes for environmental problems. *Catal. Today* **2000**, *59*, 411−416.

(11) Aerts, R.; Tu, X.; De Bie, C.; Whitehead, J. C.; Bogaerts, A. An investigation into the dominant reactions for ethylene destruction in non-thermal atmospheric plasmas. *Plasma Processes Polym.* **2012**, *9*, 994−1000.

(12) De Bie, C.; Verheyde, B.; Martens, T.; Van Dijk, J.; Paulussen, S.; Bogaerts, A. Fluid modeling of the conversion of methane into higher hydrocarbons in an atmospheric pressure dielectric barrier discharge. *Plasma Processes Polym.* **2011**, *8*, 1033−1058.

(13) Trushkin, A. N.; Kochetov, I. V. Simulation of toluene decomposition in a pulse-periodic discharge operating in a mixture of molecular nitrogen and oxygen. *Plasma Phys. Rep.* **2012**, *38*, 407−431.

(14) Magne, L.; Pasquiers, S.; Blin-Simiand, N.; Postel, C. Production and reactivity of the hydroxyl radical in homogeneous high pressure plasmas of atmospheric gases containing traces of light olefins. *J. Phys. D: Appl. Phys.* **2007**, *40*, 3112−3127.

(15) Tu, X.; Whitehead, J. C. Plasma-catalytic dry reforming of methane in an atmospheric dielectric barrier discharge: Understanding the synergistic effect at low temperature. *Appl. Catal., B* **2012**, *125*, 439−448.

(16) Sathiamoorthy, G.; Kalyana, S.; Finney, W. C.; Clark, R. J.; Locke, B. R. Chemical reaction kinetics and reactor modeling of NO_x removal in a pulsed streamer corona discharge reactor. *Ind. Eng. Chem. Res.* **1999**, *38*, 1844−1855.

(17) Evans, D.; Rosocha, L. A.; Anderson, G. K.; Coogan, J. J.; Kushner, M. J. Plasma remediation of trichloroethylene in silent discharge plasmas. *J. Appl. Phys.* **1993**, *74*, 5378.

(18) Koeta, O.; Blin-Simiand, N.; Faider, W.; Pasquiers, S.; Bary, a.; Jorand, F. Decomposition of Acetaldehyde in Atmospheric Pressure Filamentary Nitrogen Plasma. *Plasma Chem. Plasma Process.* **2012**, *32*, 991−1023.

(19) Blin-Simiand, N.; Pasquiers, S.; Jorand, F.; Postel, C.; Vacher, J.-R. Removal of formaldehyde in nitrogen and in dry air by a DBD: importance of temperature and role of nitrogen metastable states. *J. Phys. D: Appl. Phys.* **2009**, *42*, 122003.

(20) Tu, X.; Gallon, H. J.; Twigg, M. V; Gorry, P. A.; Whitehead, J. C. Dry reforming of methane over a Ni/Al_2O_3 catalyst in a coaxial dielectric barrier discharge reactor. *J. Phys. D: Appl. Phys.* **2011**, *44*, 274007.

(21) Dorai, R.; Kushner, M. J. Consequences of propene and propane on plasma remediation of NO_x. *J. Appl. Phys.* **2000**, *88*, 3739−3747.

(22) Jidenko, N.; Bourgeois, E.; Borra, J. Temperature profiles in filamentary dielectric barrier discharges at atmospheric pressure. *J. Phys. D: Appl. Phys.* **2010**, *43*, 295203.

(23) Motret, O.; Hibert, C.; Pellerin, S.; Pouvesle, J. M. Rotational temperature measurements in atmospheric pulsed dielectric barrier discharge - gas temperature and molecular fraction effects. *J. Phys. D: Appl. Phys.* **2000**, *33*, 1493−1498.

(24) Aerts, R.; Martens, T.; Bogaerts, A. Influence of vibrational states on CO_2 splitting by dielectric barrier discharges. *J. Phys. Chem. C* **2012**, *116*, 23257−23273.

(25) Van Gaens, W.; Bogaerts, A. Kinetic modelling for an atmospheric pressure argon plasma jet in humid air. *J. Phys. D: Appl. Phys.* **2013**.

(26) A. Kossyi, I.; Yu Kostinsky, A.; A. Matveyev, A.; V. Silakov, P. Kinetic scheme of the non-equilibrium discharge in nitrogen-oxygen mixtures. *Plasma Sources Sci. Technol.* **1992**, *1*, 207−220.

(27) Snoeckx, R.; Aerts, R.; Tu, X.; Bogaerts, A. Plasma-based dry reforming: A computational study ranging from nanoseconds to seconds timescale. *J. Phys. Chem. C* **2013**.

(28) Fridman, A. *Plasma Chemistry*; Cambridge University Press: New York, 2008.

(29) Nielsen, R.; Bradbury, N. Electron and negative ion mobilities in oxygen, air, nitrous oxide and ammonia. *Phys. Rev.* **1937**, *51*, 69−75.

(30) Tu, X.; Verheyde, B.; Corthals, S.; Paulussen, S.; Sels, B. F. Effect of packing solid material on characteristics of helium dielectric barrier discharge at atmospheric pressure. *Phys. Plasmas* **2011**, *18*, 080702.

(31) Plessis, P.; Marmet, P. Electroionization study of acetylene and fragment ions. *Int. J. Mass Spectrom. Ion Processes* **1986**, *70*, 23−44.

(32) Baulch, D. L.; Cobos, C. J.; Cox, R. A.; Esser, C.; Frank, P.; Just, T.; Kerr, J. A.; Pilling, M. J.; Troe, J.; Walker, R. W.; Warnatz, J. Evaluated kinetic data for combustion modelling. *J. Phys. Chem. Ref. Data* **1992**, *21*, 411−734.

(33) Baulch, D. L. Evaluated kinetic data for combustion modeling: Supplement II. *J. Phys. Chem. Ref. Data* **2005**, *34*, 757.

(34) Hübner, M.; Röpcke, J. On the destruction of volatile organic compounds using a dielectric pellet bed reactor. *J. Phys. (Paris)* **2009**, *157*, 012004.

(35) Kushner, M. J. Destruction mechanisms temperature plasmas for formaldehyde in atmospheric pressure low. *J. Appl. Phys.* **1993**, *73*, 51−55.

(36) Liang, W.-J.; Li, J.; Li, J.-X.; Zhu, T.; Jin, Y.-Q. Formaldehyde removal from gas streams by means of $NaNO_2$ dielectric barrier discharge plasma. *J. Hazard. Mater.* **2010**, *175*, 1090−5.
(37) Atkinson, R.; Aschmann, S. M.; Pitts, J. N. Rate constants for the gas-phase reactions of the nitrate radical with a series of organic compounds at 296 ± 2 K. *J. Phys. Chem.* **1988**, *92*, 3454−3457.
(38) Dunlea, E. J.; Talukdar, R. K. Ravishankara, a R. Kinetic studies of the reactions of $O_2(b^1\sum_g^+)$ with several atmospheric molecules. *J. Phys. Chem. A* **2005**, *109*, 3912−3920.
(39) Zhu, A.-M.; Sun, Q.; Niu, J.-H.; Xu, Y.; Song, Z.-M. Conversion of NO in NO/N_2, $NO/O_2/N_2$, $NO/C_2H_4/N_2$ and $NO/C_2H_4/O_2/N_2$ systems by dielectric barrier discharge plasmas. *Plasma Chem. Plasma Processing* **2005**, *25*, 371−386.
(40) Eliasson, B.; Hirth, M.; Kogelschatz, U. Ozone synthesis from oxygen in dielectric barrier discharges. *J. Phys. D: Appl. Phys.* **1987**, *20*, 1421−1437.
(41) Kogelschatz, U.; Eliasson, B.; Egli, W. Dielectric-barrier discharges. principle and applications. *J. Phys. IV* **1997**, *07*, C4−47−C4−66.
(42) Atkinson, R.; Baulch, D. L.; Cox, R. A.; Crowley, J. N.; Hampson, R. F.; Hynes, R. G.; Jenkin, M. E.; Rossi, M. J.; Troe, J. Evaluated kinetic and photochemical data for atmospheric chemistry: Volume I - gas phase reactions of O_x, HO_x, NO_x and SO_x species. *Atmos. Chem. Phys.* **2004**, *4*, 1461−1738.
(43) Person, J. C.; H., D. O. Removal of SO_2 and NO(x) from stack gases by electron beam irradiation. *Radiat. Phys. Chem.* **1988**, *31*, 1−8.
(44) Atkinson, R.; Baulch, D. L.; Cox, R. A.; Hampson, R. F.; Kerr, J. A.; Rossi, M. J.; Troe, J. Evaluated kinetic and photochemical data for atmospheric chemistry: Supplement VI. IUPAC subcommittee on gas kinetic data evaluation for atmospheric chemistry. *J. Phys. Chem. Ref. Data* **1997**, *26*, 1329−1499.
(45) Forster, P.; Ramaswamy, V.; Artaxo, P.; Berntsen, T.; Betts, R.; Fahey, D. W.; Haywood, J.; Lean, J.; Lowe, D. C., Myhre, G.; Nganga, J.; Prinn, R.; Raga, G.; Schulz, M.; Van Dorland, R. Changes in atmospheric constituents and in radiative forcing. In: Solomon, S., Qin, D., Manning, M., Eds. *Climate Change 2007: the Physical Science Basis, Contribution of Working Group I to the Fourth Assessment Report of the Intergovernmental Panel on Climate Change*; Cambridge University Press: New York, 2007.